World Academy of Science, Engineering and Technology
International Journal of Physical and Mathematical Sciences
Vol:7, No:7, 2013

The Influence of Gravity on The Temporal Instability of Viscoelastic Liquid Curved Jets

Abdullah Madhi Alsharif and Jamal Uddin

***Abstract*—** A liquid curved jet has many applications in different industrial and engineering processes, such as the prilling process for generating small spherical pellets (fertilizer or magnesium). The liquids used are usually molten and contain small quantities of polymers and therefore can be modelled as non-Newtonian liquids. In this paper, we model the viscoelastic liquid jet by using the Oldroyd-B model. An asymptotic analysis has been used to simplify the governing equations. Furthermore, the trajectory and a linear temporal stability in the presence of gravity and rotation have been determined.

***Keywords*—** gravity, prilling, rotation, viscoelastic jets.

I. Introduction

IT is important to understand the behaviour of non-Newtonian jets because this phenomena of viscoelastic jets has many industrial applications, including ink jets, fertilizers, roll coating and paint levelling. Lord Rayleigh [19] carried out the theoretical treatment for the instability of incompressible inviscid liquid jets and found that the reason for break-up is the surface tension. He found that the maximum growth happens at $ka = 0.697$ with a corresponding wavelength $\omega \approx 2\pi R/0.697 \approx 9R$. The viscosity was considered in the cylinder of incompressible liquid jets by Weber [26] who found that the wave length of most unstable liquids is increased by the viscosity. The asymptotic theory has been applied by Papageorgiou [17] to the system of dynamics of viscous fluid jets to derive the model for the nonlinear solution. He also found that there are good agreements between theoretical and asymptotic solution. Newtonian jet stability was examined by Grant and Middleman [11] in terms of predicting the stability in turbulent and laminar jets which emerged from a nozzle. The temporal instability of capillary liquid jets was investigated by Ashgriz and Mashayek [2].

The work of Wallwork et al. [25] examines the trajectory and stability of inviscid curved liquid jets; their investigation revealed temporal and spatial stability in the case of steady state solutions. They also conducted some experiments for inviscid rotating liquid jets and found agreement between the theoretical and experimental work. Decent et al. [7] extended the previous work to include gravity in the examination of linear stability by Wallwork [24]. Moreover, the influence of viscosity on the trajectory and stability of the break-up of rotating liquid jets has been examined by Decent et al. [8] and the experiments agree with the theoretical work. However, Uddin and Decent [23] studied the instability of non-Newtonian liquid curved jets under gravity. Uddin [22] has also investigated the influence of gravity on non-Newtonian liquid curved jets by adding surfactants. The influence of gravity on the capillary jet instability was investigated by Cheong et al. [3]. They conducted experiments for this simulation and found that the increase in gravity decreases disturbance frequency and, without including gravity, the maximum wave number is $k = 0.697$, which agrees with Rayleigh's result. A numerical study has been used by Renardy [20] to find the break-up of Newtonian case and viscoelastic liquid jets for the Giesekus model and upper convected Maxwell model. The stability of viscoelastic jets has been discussed by Middleman [15] who predicted a lower stability compared to Newtonian liquid jets. This was also investigated by Goldin et al. [10], who found that the droplets of viscoelastic jets connected to threads which are thin because of the effects of stress on the thread and surface tension. Mageda and Larson [14] have used the Oldroyd-B model for ideal elastic liquids, called Boger fluids, for investigating the rheological behavior of polyisobutylene and polystyrene when the shear rates are low. Larson [12] wrote an article reviewing instability in viscoelastic flows, in which he described the simplest model for studying the viscoelastic jets, which is the Oldroyd-B model. Larson [12] also illustrated the linear and nonlinear instability for Newtonian and non-Newtonian fluids. The numerical study for pendant drop formation of viscoelastic liquid jets in air which emerged from a nozzle was examined by Davidson et al. [6]. They used Oldroyd-B model and compared the drop shapes numerically with experimental work. Cooper-White et al. [5] investigated the effects on elasticity of the drop liquid jet caused by gravity. The beads-on-string structure of viscoelastic threads was discussed by Clasen et al. [4]. They applied the Oldroyd-B model to this problem to study the beads-on-string and liquid bridge. This article is well-presented and explains the theoretical analysis and experimental study. Renardy [21] studied the linear stability of viscoelastic shear flow when the limit of high Weissenberg and Reynolds numbers by using Maxwell upper convected fluid. Liu and Liu [13] discussed the temporal instability of viscoelastic liquid jets for axisymmetric and asymmetric disturbances. The dynamics of the beads-on-a-string structure and filament thread have been discussed by Ardekani et al. [1] for weakly viscoelastic jets by using the Giesekus constitutive equation and compared the results to those of the Oldroyd-B model (when $\alpha = 0$). They found that the mobility factor α, has an influence on the neck of droplets. Morrison et al. [16] studied the viscoelasticity of the drop of ink jet which emerged from the nozzle.

School of Mathematics, The University of Birmingham. Edgbaston, Birmingham. B15 2TT. United Kingdom
Corresponding author, Email:alsharif@maths.bham.ac.uk

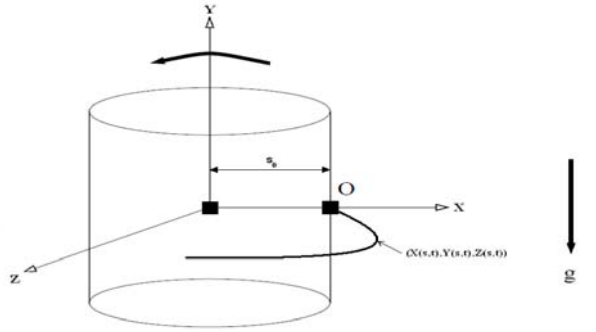

Fig. 1. Sketch of coordinate system which uses the X, Y, Z axis. O represents the orifice from which the liquid emerges.

II. Problem Formulation

We assume that a large cylindrical container has radius s_0 and rotates with angular velocity Ω. This container has a small orifice at the bottom with radius a. This radius is very small compared with the radius of the container. This problem is examined by choosing a coordinate system (X, Y, Z) rotating with the container, and having an origin at the axis of the container. The position of the orifice is at $(s_0, 0, 0)$ as shown in Fig. 1. Due to the rotation of the container, the liquid leaves the orifice in a curve. In this problem of the prilling process. The jet moves in the $(X, , Y, Z)$ plane, so that the centerline can be described by coordinates $(X(s,t), Y(s,t), Z(s,t))$, where s is the arc-length along the middle of the jet which emerges from the orifice and t is the time (see Wallwork [24]). In any cross-section of the jet we also have plane polar coordinates (n, ϕ), which are the radial and azimuthal direction and have unit vectors which are $\mathbf{e_s}$, $\mathbf{e_n}, \mathbf{e}_\phi$ (see Decent *et al*. [7]). The velocity components for this problem are $(\boldsymbol{u}, \boldsymbol{v}, \boldsymbol{w})$, where $\boldsymbol{u}$ is the tangential velocity, $\boldsymbol{v}$ is the radial velocity and $\boldsymbol{w}$ is the azimuthal velocity.

To describe the flow we have to determine the equations of motion, which are the continuity equation, the momentum equation and the constitutive equation. We used the Oldroyd-B model to study the viscoelastic liquid jet. The equations of motion take the form

$$\boldsymbol{\nabla}.\boldsymbol{u} = 0, \tag{1}$$

$$\rho\left(\frac{\partial \boldsymbol{u}}{\partial t} + \boldsymbol{u}.\boldsymbol{\nabla}\boldsymbol{u}\right) = -\boldsymbol{\nabla}p + g + \boldsymbol{\nabla}.\boldsymbol{\tau} - 2\,\boldsymbol{w}\times\boldsymbol{u} - \boldsymbol{w}\times(\boldsymbol{w}\times\boldsymbol{r}), \tag{2}$$

$$\boldsymbol{\tau} = \mu_s\left(\boldsymbol{\nabla}\boldsymbol{u} + (\boldsymbol{\nabla}\boldsymbol{u})^T\right) + T, \tag{3}$$

$$\lambda T^{\nabla} + T = \mu_p\gamma, \tag{4}$$

$$\frac{\partial T}{\partial t} + (\boldsymbol{u}.\boldsymbol{\nabla})T - T.\boldsymbol{\nabla}\boldsymbol{u} - (\boldsymbol{\nabla}\boldsymbol{u})^T.T = \frac{1}{\lambda}(\mu_p\gamma - T), \tag{5}$$

where ρ, p, μ_s, μ_p and T are the density, the pressure, the viscosity of the solvent, the viscosity of the polymer and the extra stress tensor respectively. We have two boundary conditions which are the kinematic condition which takes the form

$$\frac{\partial R}{\partial t} + u.\nabla R = 0, \text{on } n = R(s,\phi,t), \tag{6}$$

and the dynamic condition which is

$$\boldsymbol{n}.\boldsymbol{\Pi}.\boldsymbol{n} = \sigma\kappa, \text{ and } \boldsymbol{t_i}.\boldsymbol{\Pi}.\boldsymbol{n} = \boldsymbol{t_i}\cdot\nabla\sigma, \tag{7}$$

and the arc-length condition is

$$X_s^2 + Y_s^2 + Z_s^2 = 1,$$

where $\boldsymbol{\Pi} = -p\boldsymbol{I} + \boldsymbol{\tau}$, $\boldsymbol{n}$ and $\boldsymbol{t_i}$ for $i = 1$ and 2 are the total stress tensor, the unit normal and tangential vectors and σ is the surface tension of the liquid.
These equations are similar to Decent et al. [7]. However, the differences are in the equations of the extra-stress term which is T.

III. Asymptotic analysis

We expand u, v, w, p in Taylor series in ϵn (see Eggers [9]) and $R, X, Z, T_{ss}, T_{nn}, T_{\phi\phi}, T_{sn}, T_{s\phi}, T_{n\phi}$ in ϵ.

$$\begin{aligned}
&(u,v,w)(s,n,\phi,t) = (u_0,0,0)(s,t) + \\
&\qquad (\epsilon\, n)(u_1,v_1,w_1)(s,\phi,t) + ... \\
&p(s,n,\phi,t) = p_0(s,\phi,t) + (\epsilon\, n)p_1(s,\phi,t) + ... \\
&R(s,n,\phi,t) = R_0(s,t) + (\epsilon)R_1(s,\phi,t) + ... \\
&(X,Y,Z)(s,n,\phi,t) = (X_0,Y_0,Z_0)(s) + \\
&(\epsilon)(X_1,Y_1,Z_1)(s,t) + ... \\
&(T_{ss},T_{nn},T_{\phi\phi})(s,n,\phi,t) = (T^0_{ss},T^0_{nn},T^0_{\phi\phi})(s,t) + \\
&\qquad \epsilon\,(T^1_{ss},T^1_{nn},\epsilon T^1_{\phi\phi})(s,t) + ... \\
&(T_{sn},T_{s\phi},T_{n\phi})(s,n,\phi,t) = \epsilon\,(T^1_{ss},T^1_{nn},\epsilon T^1_{\phi\phi})(s,t) + ...
\end{aligned}$$

We substitute these asymptotic expansions in the equations of motion. We can therefore find from the equation of continuity at the leading order

$$v_1 = -\frac{u_{0s}}{2}. \tag{8}$$

It can be also obtained that from the equation of motion in s-direction at leading order

$$u_{0t} + u_0u_{0s} = -\frac{1}{We}\left(\frac{1}{R_0}\right)_s + \frac{(X+1)X_s + ZZ_s}{Rb^2} + \frac{3\alpha_s}{R_0^2\,Re}\left(R_0^2\,u_{0s}\right)_s - \frac{Y_s}{F^2} + \frac{1}{R_0^2Re}\left(R_0^2(T^0_{ss} - T^0_{nn})\right)_s, \tag{9}$$

$$(X_{ss}^2 + Y_{ss}^2 + Z_{ss}^2)\left(u_0^2 - \frac{3\alpha_s}{Re}\,u_{0s} - \frac{\sqrt{u}}{We}\right) = -\frac{Y_{ss}}{F^2} + \frac{2}{Rb}\,u_0\left(X_sZ_{ss} - Z_sX_{ss}\right) + \frac{(X+1)X_{ss} + ZZ_{ss}}{Rb^2} = 0, \tag{10}$$

$$\frac{Z_sX_{ss} - Z_{ss}X_s}{F^2} + \frac{(X+1)(Y_{ss}Z_s - Y_sZ_{ss})}{Rb^2} - \frac{2Y_{ss}u_0}{Rb} + \frac{Z(Y_sX_{ss} - Y_{ss}X_s)}{Rb^2} = 0, \tag{11}$$

from the extra stress tensor (Eq. 5) at leading order, we get

$$\frac{\partial T^0_{ss}}{\partial t} + u_0 \frac{\partial T^0_{ss}}{\partial s} - 2\frac{\partial u_0}{\partial s} T^0_{ss} = \frac{1}{De}\left(2(1-\alpha_s)\frac{\partial u_0}{\partial s} - T^0_{ss}\right), \quad (12)$$

$$\frac{\partial T^0_{nn}}{\partial t} + u_0 \frac{\partial T^0_{nn}}{\partial s} + \frac{\partial u_0}{\partial s} T^0_{nn} = \frac{-1}{De}\left((1-\alpha_s)\frac{\partial u_0}{\partial s} + T^0_{nn}\right), \quad (13)$$

from the kinematic condition, we obtain at ϵ

$$\frac{\partial R_0}{\partial t} + u_0 R_{0s} + \frac{R_0}{2} u_{0s} = 0, \quad (14)$$

where $Re = \frac{\rho U a}{\mu_0}$, $We = \frac{\rho U^2 a}{\sigma}$, $Rb = \frac{U}{s_0 \Omega}$, $De = \frac{\lambda U}{s_0}$ and $F = \frac{U}{\sqrt{g s_0}}$ and $\alpha_s = \frac{\mu_s}{\mu_s + \mu_p}$ are Reynolds number, Weber number, Rossby number, Deborah number, Froude number and the viscosity ratio respectively. We can see that when $Rb \to \infty$ and $F \to \infty$ the equations (9)-(14) are the same as the equations which are derived by Clasen et al. [4].

IV. Steady State Solutions

We have the governing equations for this system as

$$u_0 u_{0s} = -\frac{u_{0s}}{2We\sqrt{u}} + \frac{(X+1)X_s + ZZ_s}{Rb^2} + \frac{3\alpha_s}{Re}\left(u_{0ss} - \frac{u^2_{0s}}{u_0}\right) - \frac{Y_s}{F^2} + \frac{1}{Re}\left(\frac{\partial}{\partial s}(T^0_{ss} - T^0_{nn}) - \frac{u_{0s}}{u_0}(T^0_{ss} - T^0_{nn})\right), \quad (15)$$

$$(X^2_{ss} + Y^2_{ss} + Z^2_{ss})\left(u_0^2 - \frac{3}{Re}u_{0s} - \frac{\sqrt{u}}{We}\right) = -\frac{Y_{ss}}{F^2} + \frac{2}{Rb}u_0(X_s Z_{ss} - Z_s X_{ss}) + \frac{(X+1)X_{ss} + ZZ_{ss}}{Rb^2} = 0, \quad (16)$$

$$u_0 \frac{\partial T^0_{ss}}{\partial s} - 2\frac{\partial u_0}{\partial s} T^0_{ss} = \frac{1}{De}\left(2(\alpha_s - 1)\frac{\partial u_0}{\partial s} - T^0_{ss}\right), \quad (17)$$

$$u_0 \frac{\partial T^0_{nn}}{\partial s} + \frac{\partial u_0}{\partial s} T^0_{nn} = \frac{-1}{De}\left((\alpha_s - 1)\frac{\partial u_0}{\partial s} + T^0_{nn}\right), \quad (18)$$

$$\frac{Z_s X_{ss} - Z_{ss} X_s}{F^2} - \frac{2Y_{ss}u_0}{Rb} + \frac{(X+1)(Y_{ss}Z_s - Y_s Z_{ss})}{Rb^2} + \frac{Z(Y_s X_{ss} - Y_{ss} X_s)}{Rb^2} = 0, \quad (19)$$

and finally the arc-length condition is

$$X_s^2 + Y_s^2 + Z_s^2 = 1. \quad (20)$$

These are a system of six equations in six unknowns which are X, Y, Z, u_0, T^0_{ss} and T^0_{nn}. We solve these equations by using the Runge-Kutta method in the inviscid limit (see parau et al. [18]) for obtaining the trajectory of the jet with following initial conditions as $u_0(0) = R_0(0) = X_s(0) = 1$ and $Y(0) = X(0) = Z(0) = Z_s(0) = Y_s(0) = 0$. In Figs. 2 and 3 show the influence of changing the Froude number and the Rossby number on the trajectory of a viscoelastic liquid jet, which means when we decrease the Froude number the effect of gravity becomes stronger on the trajectory. We find the relationship between the extra stress tensor,T^0_{ss} and T^0_{nn} and the arc-length s for different values of Rossby number and Froude number which are in Figs. 4-7.

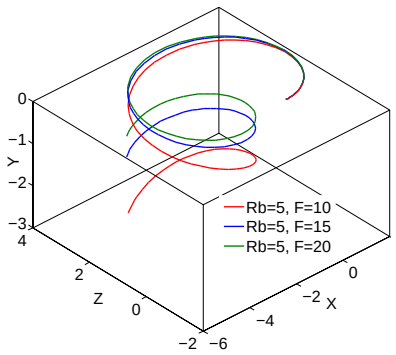

Fig. 2. Graph showing the trajectory of a liquid jet under the effect of gravity and rotation for different values of the Froude number where $De = 15$ and $\tilde{\alpha} = 20$.

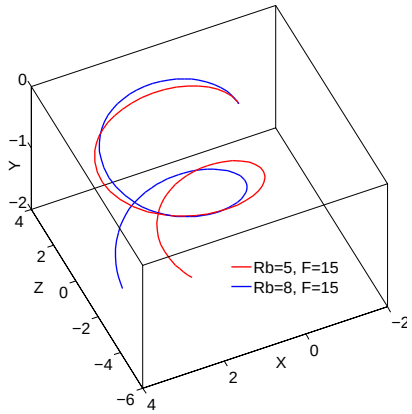

Fig. 3. Graph showing the trajectory of a rotating liquid jet under the effect of gravity and rotation for different values of the Rossby number where $De = 15$ and $\tilde{\alpha} = 20$.

V. Linear Temporal Instability Analysis

We now consider the travelling wave modes of the form $exp(ik\bar{s} + \bar{t})$, where $\bar{s} = s/\epsilon$ is small length scales, $\bar{t} = t/\epsilon$ is small time scales, $k = k(s)$ and $\omega = \omega(s)$ are the wavenumber and frequency of the disturbances, and δ is a small constant which is $0 < \delta < \epsilon^2$ (see Uddin [22]).

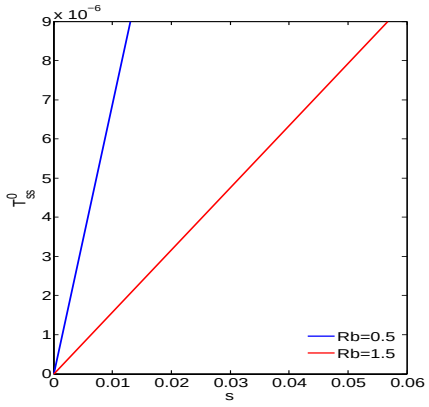

Fig. 4. Graph showing the relationship between T^0_{ss} and arc-length s of a rotating liquid jets under the effect of gravity for different values of the Rossby number at $F = 3$ and $We = 25$at $De = 15$ and $\tilde{\alpha} = 20$.

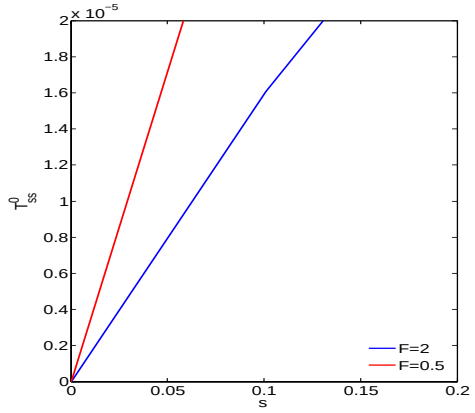

Fig. 6. Graph showing the relationship between T^0_{ss} and arc-length s of a rotating liquid jets under the effect of gravity for different values of the Froude number at $Rb = 1.5$ and $We = 25$ where $De = 15$ and $\tilde{\alpha} = 20$.

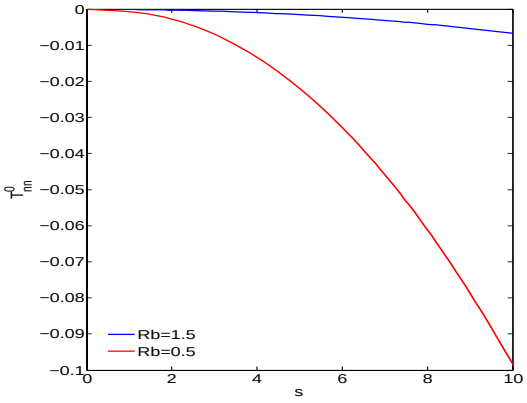

Fig. 5. Graph showing the relationship between T^0_{nn} and arc-length s of a rotating liquid jet under the effect of gravity for different values of the Rossby number at $F = 3$ and $We = 25$ at $De = 15$ and $\tilde{\alpha} = 20$.

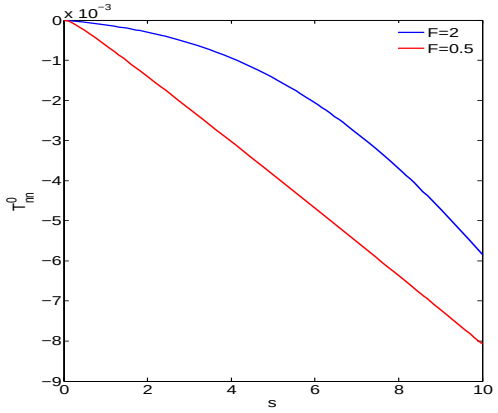

Fig. 7. Graph showing the relationship between T^0_{nn} and arc-length s of a rotating liquid jet under the effect of gravity for different values of the Froude number at $Rb = 1.5$ and $We = 25$, where $De = 15$ and $\tilde{\alpha} = 20$.

We make small perturbations to the steady state solutions having the form $\delta\, exp(ik\bar{s}+\bar{t})$, where δ is a small dimensionless constant. Then we obtain the eigenvalue relation at the leading order which has the form

$$\left(\omega + iku_0\right)^2 + \frac{3\tilde{\alpha_s}k^2}{Re}\left(\omega + iku_0\right) - \frac{k^2R_0}{2We}\left(\left(\frac{1}{R_0^2} - k^2\right) - \frac{2We}{R_0\,Re}(T^0_{ss} - T^0_{nn})\right) - \frac{k^2}{Re}\left(2T^0_{ss} + T^0_{nn} + \frac{3}{De}\right) = 0. \quad (21)$$

There is a new scaling for the viscosity ratio which is $\tilde{\alpha_s} = \frac{\alpha_s}{\epsilon}$. Without this new scaling, we cannot bring the viscous term into the equations which derived the dispersion relation. As we mentioned earlier, $\alpha_s + \alpha_p = 1$, where α_s and α_p are the solvent viscosity and the polymeric viscosity respectively. After substituting the new scaling, the last equation becomes $\epsilon\tilde{\alpha_s} + \alpha_p = 1$, which means that $\alpha_p \gg \alpha_s$. However, both the solvent viscosity and the polymeric viscosity are very small. By choosing $\omega_i = -ku_0$, and differentiating the last equation with respect of k we get

$$k^* = \frac{1}{(2R_0^3)^{1/4}} \frac{\left(\frac{R_0GWe}{2} + 1 - 2B\right)^{\frac{1}{2}}}{\sqrt{\left(3\tilde{\alpha_s}Oh + \sqrt{2R_0}\right)}}, \quad (22)$$

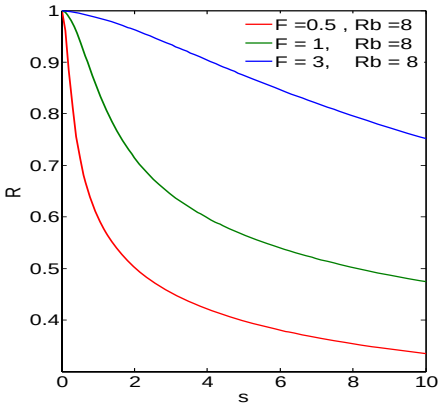

Fig. 8. Graph showing the relationship between the radius and the arc-length s for different values of the Froude number and the Rossby number when $We = 15$.

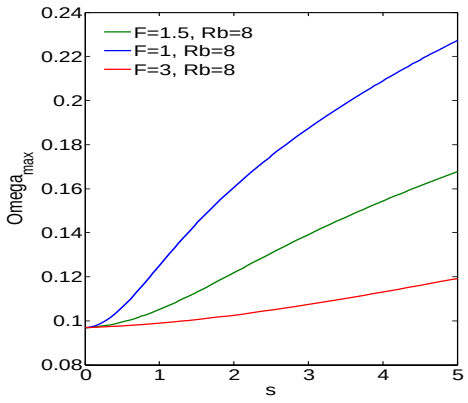

Fig. 9. Graph showing the relationship between the growth rate ω_r^* of the most unstable mode against the arc-length s for a viscoelastic liquid jet, where the dimensionless numbers are $Re = 1000, We = 10, De = 15, \tilde{\alpha} = 20$.

where $B = T_{ss}^0 - T_{nn}^0$ and $G = \frac{4}{Re}\left(2T_{ss}^0 + T_{nn}^0 + \frac{3}{De}\right)$. For temporal instability, the growth rate ω_r is positive, which happens when $0 < kR < 1$ where $k = k^*$, and R_0 is found from the steady state solutions.

VI. Results

In this section we examine the linear stability of disturbances about the steady state solutions obtained in the last section. It can be noticed in Fig. 8 that the radius of the jet decreases with an increasing arc-length s. This Fig. also shows that when the Froude number increases with the constant Rossby number, $F = 0.5, 1$ and 3, $Rb = 8$, the radius of the jet increases, which means the liquid jet becomes thinner and moves more slowly. In Figs. 9 and 10, we plot the correlation between the growth rate and the wavenumber of the most unstable modes and the arc-length for different values of Froude number.

In Fig. 11, we chose a different value of the Rossby number, making the Froude number as a constant, and showing that when we increase the Rossby number the radius of the jet increases as well. The same procedure is applied in Figs. 12 and 13 to find the relationship between the growth rate and the most unstable mode for the wavenumber and arc-length s. It can also be seen that when the Rossby number increases the growth rate and the wavenumber increases.

VII. Conclusion

We have discussed the linear stability of a viscoelastic liquid jets falling under gravity and rotation rates. We therefore have examined the most unstable mode and growth rate for viscoelastic liquid jets and found that a linear mode varies with the distance downstream of the jet. This linear stability cannot predict the satellite droplets. However, the main droplet sizes for this prilling process can be predicted.

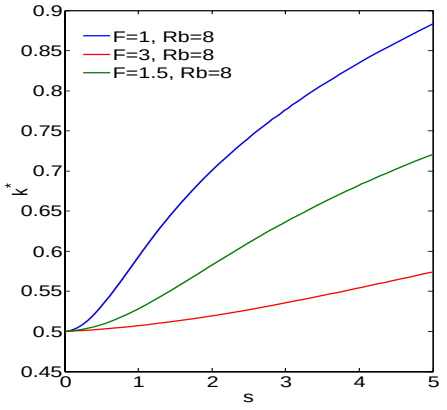

Fig. 10. Graph showing the relationship between the most unstable mode k^* and the arc-length s for a viscoelastic liquid jet, where the dimensionless numbers are $Re = 1000, We = 10, De = 15, \tilde{\alpha} = 20$.

Acknowledgment

The author would like to thank Taif University for their financial support.

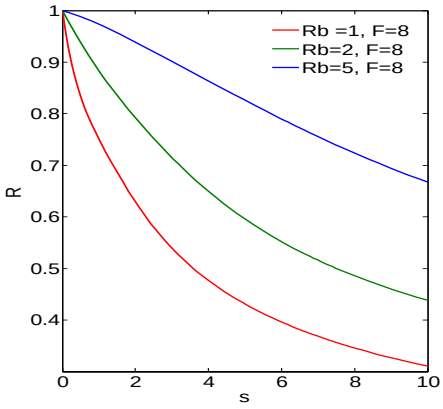

Fig. 11. Graph showing the relationship between the radius and the arc-length s for different values of the Froude number and the Rossby number when $We = 15$.

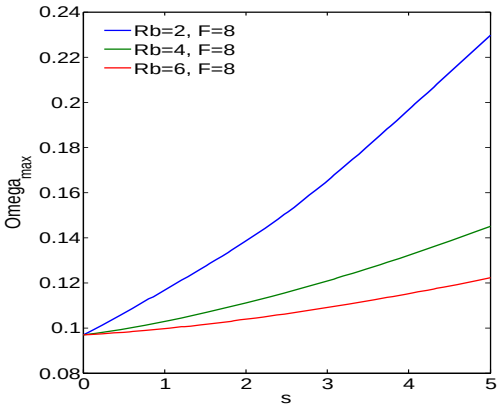

Fig. 12. Graph showing the relationship between the growth rate ω_r^* of the most unstable mode against the arc-length s for a viscoelastic liquid jet, where the dimensionless numbers are $Re = 1000, We = 10, De = 15, \tilde{\alpha} = 20$.

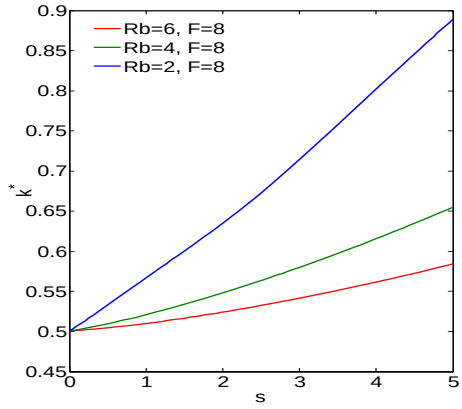

Fig. 13. Graph showing the relationship between the most unstable mode k^* and the arc-length s for a viscoelastic liquid jet, where the dimensionless numbers are $Re = 1000, We = 10, De = 15, \tilde{\alpha} = 20$.

REFERENCES

[1] Ardekani, A. M., Sharma, V., and Mckinley, G. H., 2010, Dynamics of bead formation, filament thinning and breakup in weakly viscoelastic jets. J. Fluid Mech. 665, 46-56
[2] Ashgriz, N. and Mashayek, F., 1995. Temporal analysis of capillary jet breakup. J. Fluid Mech. 291, 163-190.
[3] Cheong, B. S., Howes, T., 2004, Capillary jet instability under influence of gravity, Chemmical Engineering Science, 59, 2145-2157
[4] Clasen, C., Eggers, J., Fonlelos, M. A., Li, j., and Mckinley, G. H., 2006, The beads-on-string structure of viscoelastic threads. J. Fluid Mech., 556, 283-308
[5] Cooper-White, J. J., Fagan, J. E., Tirtaatmadja, V., Lastert, D. R., and Boger, D. V., 2002, Drop formation dynamics of constant low-viscosity, elastic fluids, J. Non-Newtonian fluid Mech., 106,29-59
[6] Davidson, M. R., Harvie, J. E., and Cooper-White, J. J., 2006, Simulation of pendant drop formation of a viscoelastic liquid, Korea-Australia Rheology Journal, 18, (2), 41-49
[7] Decent, S. P., King, A. C. and Wallwork, I. M., 2002, Free jets spun from a prilling tower, Journal of Engineering Mathematics, 42, 265-282
[8] Decent, S. P., King, A. C., Simmons, M. H., Părău, E. I., Wong, D. C. Y., Wallwork, I. M., Gurney, C., and Uddin, J., 2007, The trajectory and stability of a spiralling liquid jet: Part II. Viscous Theory, Appl. Math. Modelling, 33, (12), 4283-4302
[9] Eggers, J., 1997. Nonlinear dynamics and breakup of free surface flows. Rev. Mod. Physis, 69, (3), 865-929.
[10] Goldin, M., Yerushalmi, J., Pfeffer, R., and Shinner, R., 1969, Breakup of a viscoelastic fluid. J. Fluid Mech. 38, 689-711.
[11] Grant, R. P., and Middleman, S., 1965, Newtonian jet stability. A. I. Ch. E. Journal, 2, 669.
[12] Larson, R. G., 1992, Instabilities in viscoelastic flows, Rheol., Acta,31
[13] Liu, Z., and Liu, Z., 2008, Instability of a viscoelastic liquid jet with axisymmetric and asymmetric disturbance, International Journal of Multiphase Flow, 34, 42-60
[14] Mageda, J. J., and Larson, R. G., 1988, Atransition occurring in ideal elastic liquids during shear flow, J. Non-Newtonian Fluid Mech., 30,1-19
[15] Middleman, S., 1965, Stability of a viscoelastic jet, Chem. Eng. Sci. 20, 1037-1040.
[16] Morrison, N. F., Harlen, O. G. 2010, Viscoelasticity in inkjet printing, Rheol., Acta, 49, 619-632
[17] Papageorgiou, D. T., 1995, On the breakup of viscous liquid threads, Phys. Fluids, 7, 1529 Nonlinear travelling waves on a spiralling liquid jet, Wave Motion, 43, 599-613.
[18] Părău, E. I., Decent, S. P., Simmons, M. J. H., Wong, D. C. Y. and King, A. C., 2007, Nonlinear viscous liquid jets from a rotating orifice, J. Of Eng. Maths., 57, 159-179
[19] Rayleigh, W. S., 1878, On the instability of jets, Proc. Lond. Math. Soc 10,4.
[20] Renardy, M., 1995, A numerical study of the asymptotic evolution and breakup of Newtonian and viscoelastic jets, J. Non-Newtonian Fluid Mech., 59, 267-282
[21] Renardy, M., 2008, Stability of viscoelastic shear flows in the limit of high Weissenberg and Reynolds numbers, J. Non-Newtonian Fluid Mech., 155, 124-129
[22] Uddin, J., 2007. An investigation into methods to control breakup and droplet formation in single and compound liquid jets. PhD thesis, University of Birmingham.
[23] Uddin, J., and Decent, S. P., 2010, Instability of non-Newtonian liquid jets curved by gravity. Mathematics in industry, 15, 597-602.
[24] Wallwork, I. M., 2002a, The trajectory and stability of a spiralling liquid jet, Ph.D. Thesis, University of Birmingham, Birmingham.
[25] Wallwork, I. M., Decent, S.P., King, A. C. and Schulkes, R. M. S., 2002b, The trajectory and stability of a spiralling liquid jet. Part 1, Inviscid Theory, J. Fluid Mech., 459,43-65.
[26] Weber, C., 1931, Zum Zerfall eines Flussigkeitsstrahles. Z. Angew. Math. Mech, 11, 136-154.